



ACADÉMIE
DES SCIENCES
INSTITUT DE FRANCE

Comptes Rendus

Chimie

Clément Laskar, Amine Dakkoune, Carine Julcour, Florent Bourgeois,
Béatrice Biscans and Laurent Cassayre

Case-based analysis of mechanically-assisted leaching for hydrometallurgical extraction of critical metals from ores and wastes: application in chalcopyrite, ferronickel slag, and Ni-MH black mass


Volume 27, Special Issue S4 (2024), p. 37-52

Online since: 27 August 2024

Part of Special Issue: GDR Prométhée – French Research Network on
Hydrometallurgical Processes for Primary and Secondary Resources

Guest editors: Laurent Cassayre (CNRS-Université de Toulouse, Laboratoire de Génie Chimique, France) and Hervé Muhr (CNRS-Université de Lorraine, Laboratoire Réactions et Génie des Procédés, France)

<https://doi.org/10.5802/crchim.325>

 This article is licensed under the
CREATIVE COMMONS ATTRIBUTION 4.0 INTERNATIONAL LICENSE.
<http://creativecommons.org/licenses/by/4.0/>



*The Comptes Rendus. Chimie are a member of the
Mersenne Center for open scientific publishing*
www.centre-mersenne.org — e-ISSN : 1878-1543



Research article

GDR Prométhée – French Research Network on *Hydrometallurgical Processes for Primary and Secondary Resources*

Case-based analysis of mechanically-assisted leaching for hydrometallurgical extraction of critical metals from ores and wastes: application in chalcopyrite, ferronickel slag, and Ni-MH black mass

Clément Laskar^{*,a}, Amine Dakkoune^{*,a}, Carine Julcour^{*,a}, Florent Bourgeois^{*,a},
Béatrice Biscans^{*,a} and Laurent Cassayre^{*,a}

^a Laboratoire de Génie Chimique (LGC), Université de Toulouse, CNRS UMR 5563,
INP, UPS, 4, Allée Emile Monso, 31400 Toulouse, France
E-mail: clement.laskar@gmail.com (C. Laskar)

Abstract. The overall performance of hydrometallurgical leaching operations can be limited by the presence of various types of insoluble layers coating the surface of the treated solids. The attrition-leaching process, which is carried out in a stirred reactor containing millimetric beads, can partially overcome this problem and increase the extraction yield by physically abrading the layers. Through a comparative analysis of three different systems, this work develops a constructive discussion of the attrition-leaching process. The systems of interest are (i) mineral carbonation of ferronickel slag, (ii) dissolution of a chalcopyrite concentrate in sulfuric media, and (iii) dissolution of spent Ni-MH battery black mass powder in sulfuric media. In the case of ferronickel slag and chalcopyrite, the reaction yields are improved by a factor of 10 with attrition-leaching compared to leaching only, while there is no yield improvement in the case of Ni-MH black mass batteries, highlighting that the layers observed on the grain surface do not interfere with the leaching reaction. Despite very different system chemistries and conditions, the particle size distribution is similar for the three materials, showing that particles' behavior is controlled by the attrition environment. This work offers a simple setup for investigating the potential improvements of the kinetics and yields of leaching reaction due to concomitant attrition. It also allows a fundamental study of the physico-chemical processes involved, by testing whether a leaching reaction is hindered by an *in situ* passivation at the surface of a material.

Keywords. Mechano-chemical processing, Leaching, Passivation layer, Aqueous mineral carbonation, Ferronickel slags, Chalcopyrite, Nickel metal Ni-MH hydride batteries.

Funding. French National Research Agency project BIOMEALIX (Grant No. ANR-18-CE07-003101), project Carmex (Grant No. ANR-08-PCO2-002), New Caledonian Energy Agency ACE (Grant No. CS17-3160-00), French Environment and Energy Management Agency ADEME (Grant No. 1894C0021).

Manuscript received 20 November 2023, revised 24 June 2024, accepted 26 June 2024.

*Corresponding author

1. Introduction

Recycling, decarbonization, and energy optimization are crucial concerns for both chemical engineering and environmental conservation. Waste generation can be reduced by recovering end-of-life products (e.g., battery recycling) more efficiently and valorizing industrial and mining by-products (e.g. slags, mine tailings). Circular hydrometallurgical processes are promising solutions for these concerns [1]. Optimizing reagents consumption while achieving higher yields and faster reaction kinetics is therefore essential. In such hydrometallurgical processes, various parameters affect the efficiency of the leaching reaction [2], including the type and concentration of the leaching agent (e.g. H_2SO_4 , HCl), temperature, particle size, the agitation and the solid to liquid ratio (S/S+L). During reactions occurring at the solid–fluid interface, passivating layers may form on material surface through dissolution/precipitation mechanisms. These layers severely limit reactivity and applicability by hindering the kinetics of dissolution of materials, as they hinder the diffusion of the liquid reactant (e.g. protons) towards the unreacted core [2].

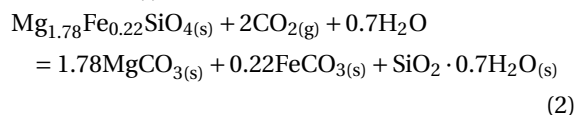
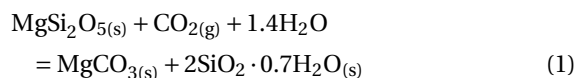
In this frame, mechano-chemical techniques play an important role in recovery of metals from wastes [3,4], as well as mineral carbonation [5], a very promising method for CO_2 storage and utilization due to its applicability to large-scale materials [6–10]. Mechanical activation of materials, achieved through attrition, amorphization and formation of new phases can, in particular, aid in increasing the reactive surface before or during leaching and enhance the dissolution rate [11].

Among the mechano-chemical processes, attrition-leaching is a promising option [12–15]. It consists in adding mm-sized beads directly in the leaching reactor, in order to intensify the leaching reaction, while improving kinetics and yield by particle grinding and *in situ* removal of leached layers. Attrition-leaching process shows synergy between two phenomena with very different timescales: attrition (time <second) and leaching of the material (time ~several hours). The attrition rate needs to be higher than the rate of passivation layer formation for an efficient depassivation on material surface. The leaching rate is related to the typical dissolution reaction time of the material, which is usually long for refractory materials. The main advantages of attrition-

leaching process are: attrition is a proven technology at large scale with slurry concentrations up to 40 wt% ($m_{\text{solid}}/m_{\text{solid}} + m_{\text{liquid}}$; S/S+L); broad feed particle size distribution, from μm to mm size range; operating at high temperature and pressure; scalability, from 4 L to 50 m^3 (e.g. IsaMill™ process [16]).

To investigate the applicability and efficiency of the attrition-leaching process, we have studied reactions of three different chemical systems where formation of layers on surface is observed during leaching (Figure 1): (i) mineral aqueous carbonation of ferronickel slag, an industrial waste produced by the primary nickel pyrometallurgical industry in New Caledonia, whose leaching is hindered by the formation of amorphous silica layers [13,14,17–20]; (ii) acid leaching of a chalcopyrite concentrate, one of the most abundant ores for copper primary production, in which Cu dissolution is inhibited by complex combined chemical and electronic phenomena [15,21,22]; (iii) dissolution of spent battery black mass powder, produced at industrial scale from nickel-metal hydride (Ni-MH) automotive batteries, whose particles exhibit a complex superposition of porous oxide layers [23], which are thought to inhibit the efficient dissolution of critical metals (Ni, Co, La, Ce) [24]. The disparity of three systems and its materials allows us to investigate the potential differences and similarities in their reactivity during the attrition-leaching process.

In these chemical systems, different types of layers can form on particles' surfaces (Figure 2). In the case of ferronickel slag, composed mainly of magnesium silicates (amorphous MgSi_2O_5 and ferrous forsterite, $\text{Mg}_{1.78}\text{Fe}_{0.22}\text{SiO}_4$, the Mg-rich endmember of the olivine solid solution series), an hydrated silica passivation layer ($\text{SiO}_2 \cdot x\text{H}_2\text{O}$) may form during the following carbonation reactions [18]:



Ferronickel slag is a promising material for mineral carbonation, as an industrial by-product [25]. However, due to the silicate layers, a dissolution plateau is reached without mechano-chemical activation, limiting the carbonation reaction [26,27].

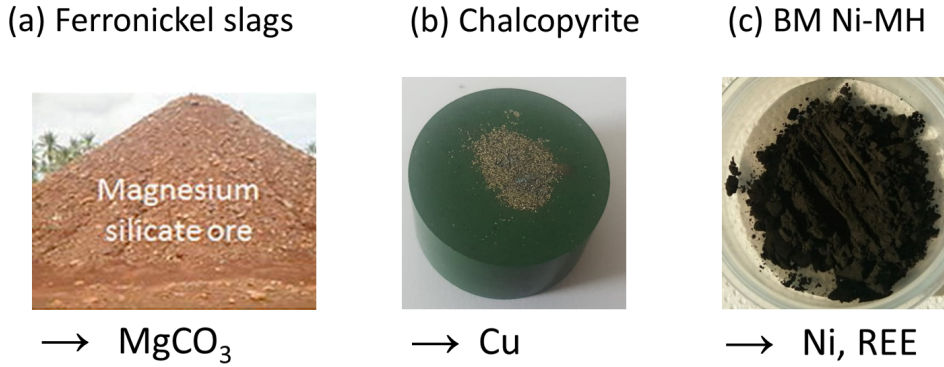


Figure 1. Systems used in this study: Ferronickel slag (a), chalcopyrite concentrate (b) and black mass of Ni-MH battery (c).

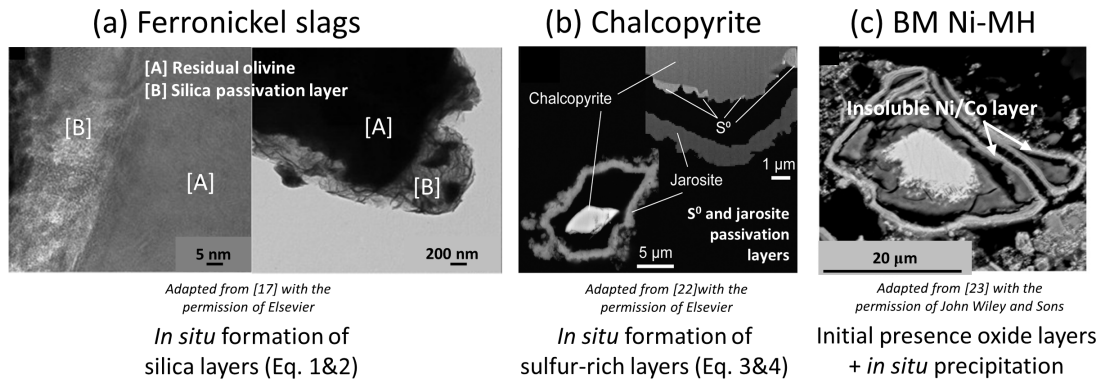
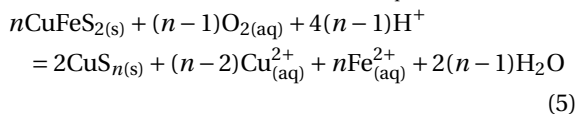
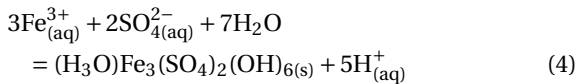
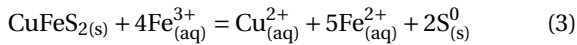


Figure 2. Respective phases and elements of interest and their chemical layers hindering the leaching reaction yields and kinetics: olivine grains ((Mg,Fe)₂SiO₄) with silica-rich (SiO₂) layers [17] (a); chalcopyrite grains (CuFeS₂) with sulfur (S⁰) and jarosite (KFe₃(SO₄)₂(OH)₆) layers [22] (b); and Ni/Co and REE (rare-earth elements) rich grains with Ni/Co insoluble layers [23] (c).

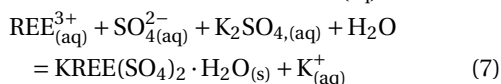
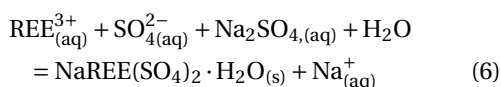
In the case of chalcopyrite (CuFeS₂), there is no consensus on the exact cause of passivation, and it is attributed to the *n*-type semiconducting nature of chalcopyrite [28], or formation of various sulfur-rich passivation layers [15]: elemental sulfur, S⁰ [29]; jarosite, KFe₃(SO₄)₂(OH)₆ [22]; copper polysulfide, CuS_{*n*} (*n* > 2; [30]), through the following reactions:



Mechano-chemical applications have been developed to optimize the chalcopyrite leaching step, which is very slow at moderate temperatures (~100 h at 75 °C; [31]): for example, by grinding the copper concentrate prior to leaching [32], or with a continuous flow between a leach tank reactor and a smaller stirred tank reactor (FLS[®] Rapid Oxidative Leach (ROL) process [33]).

In the case of black mass Ni-MH powder (BM Ni-MH), Zielinski [23] observed the presence of an insoluble Ni/Co oxide layer (62 at% Ni, 9 at% Co, <0.5 at% REE) on the surface of leached particles after 22 h in HCl solution of pH 3 at a temperature of 60 °C, while the leaching yield of Ni is not complete (<50%). This layer appears porous due to the hollow core structure

of the remaining particles after leaching. This raises a question about the effect of such layers on leaching efficiency, and whether attrition-leaching may enhance Ni dissolution. This limitation in dissolution of BM Ni-MH material for nickel has been frequently reported, with leaching yields remaining below 90% even after several hours at mildly acidic concentrations (<1 M HCl or H₂SO₄), as reported in a review by Cassayre [24]. In contrast, leaching yields of REE are rapid and high, reaching over 90% in just a few hours [24]. The limitation for REE leaching is the precipitation of these elements as double sulfate salts [24], as shown in the following reactions:



The potential limitation of Ni dissolution due to *in situ* precipitation of REE double sulfate salts has not been much investigated.

The implementation of mechano-chemical processes with mechanical activation prior to leaching has already been reported for these three systems: silicates carbonation (olivine, [34]; kimberlite and wollastonite, [35]; akermanite, [36]), copper ores leaching [32,33,37–41] and Ni-MH battery leaching [42]. However, only a few recent works have studied concomitant mechano-dissolution processes [12–15,18,20,33,36], calling further studies to identify and compare the governing mechanisms as well as the industrial feasibility for a variety of materials. Specifically, this study examines the case of BM Ni-MH dissolution, mechanically enhanced by attrition-leaching, for which leaching yields and kinetics may be improved owing to the presence of insoluble layers on the grain surface. The results obtained from the BM Ni-MH leaching experiments are compared to those obtained from previous studies with ferronickel slags [20] and chalcopyrite [15]. This comparison examines maximum dissolution yields, reaction kinetics, and physicochemical properties of the solid of these three materials, in order to provide a broader perspective of the synergistic effect of attrition-leaching and to highlight the potential of such process in materials passivation.

2. Materials and methods

2.1. Materials and chemicals

The composition of the materials used in this study is shown in Table 1.

- Ferronickel slags are a by-product of pyrometallurgical Ni extraction from New Caledonia's lateritic nickel ores (see [13] for more details). They are a mixture of ferrous forsterite (Fe_{0.22}Mg_{1.78}SiO₄) and an amorphous magnesium silicate phase (MgSi₂O₅).
- The chalcopyrite material was a flotation concentrate from the Aitik Mine in Sweden (see [15] for more details) which was homogenized and sampled using riffle splitters. This material was stored without any special precautions, which means that surface passivation due to air oxidation may have occurred. It consists of two major phases, chalcopyrite (CuFeS₂) and pyrite (FeS₂), and two minor phases, quartz (SiO₂) and molybdenite (MoS₂).
- Spent Ni-MH batteries were collected and treated by the SNAM Group and they consisted of a mixture of anodes, cathodes, and casing materials [43]. To obtain the resulting BM powder for use, these batteries were dismantled, thermolyzed in an oven and crushed by knife milling. BM was stored without any specific precautions until it was homogenized and sampled several years later using riffle splitters. It was then sieved to produce two different fractions: <100 µm and 100–500 µm. The material is a complex mixture of NiO, Ni and LaNi₅ particles. The presence of potassium (3–6 wt% K) is attributed to residual KOH electrolyte contained in the batteries.

Two types of beads were used as grinding media based on the chemistry of the aqueous solution, the operating conditions and the products to be valorized [44]: (i) glass beads (GlassBeads 1.5 type from Netzsch Group), with a density of 2.5 g/cm³, diameters between 1.2 and 1.6 mm and a chemical composition of 72.5 wt% SiO₂, 13 wt% Na₂O, 9 wt% CaO, and 4 wt% MgO; (ii) yttriated zirconia beads (Netzsch ZetaBeads Plus), with a density of 6.0 g/cm³ and a diameter of 1.0 mm. The glass beads were used for BM Ni-MH and chalcopyrite leaching to avoid

Table 1. Average chemical and mineralogical compositions of the materials

Ferronickel slag ^a											
Chemical composition (wt% as oxides)											
SiO ₂	MgO	Fe ₂ O ₃	Al ₂ O ₃	Cr ₂ O ₃	CaO	MnO					
52.6	31.2	12.4	2.7	1.1	0.7	0.2					
Phase distribution (wt%)											
Amorphous phase ^b		Mg _{1.78} Fe _{0.22} SiO ₄		FeCr ₂ O ₄		MgSiO ₃					
54–56		42–44		1.6		0.1–0.4					
Chalcopyrite ^c											
Elemental composition (wt%)											
Fe	Cu	Si	Al	K	Na	Zn	Mo	Ca	S _{SO₄}	S _{sulfide}	S ⁰
30.60	28.57	2.90 ±	0.83 ±	0.37 ±	0.21 ±	0.25 ±	0.17 ±	0.13 ±	0.21 ±	33.27	0.01 ±
± 0.17	± 0.23	0.20	0.05	0.02	0.02	0.01	0.01	0.01	0.01	± 0.32	0.01
Phase distribution (wt%)											
CuFeS ₂	FeS ₂	SiO ₂	MoS ₂	KAlSi ₃ O ₈	NaAlSi ₃ O ₈	Fe ₃ O ₄					
76.72	11.88	2.83	0.28	2.63	2.43	2.38					
BM Ni-MH											
Elemental composition (wt%)											
		Ni	La	K	Na	Co	Ce	Fe	Al		
	<100 μm	45 ± 5 ^d	8.6 ± 1.8 ^d	5.2 ± 2.1 ^d	1.0	5.6	3.7	0.53	0.14		
	100–500 μm	47	10.8	3.6	0.31	— ^f	— ^f	— ^f	— ^f		
Main phases ^e		Ni, NiO, CeO ₂ , graphite									
Minor phases ^e		Co ₃ La ₂ , La ₇ Ni ₁₆									

^aData taken from [20].^bAmorphous phase is mainly composed of amorphous MgSiO₅ [18].^cData taken from [15].^dUncertainties are derived from the standard deviation of a set of 5 samples, demonstrating the light inhomogeneity of this material due to the low amount used (0.2 g) for mineralization.^eAccording to [23].^f“—” means not measured.

breaking the glass reactor used to process these materials. The potential reactivity of the beads was also evaluated. Zirconia beads were used instead of glass beads in ferronickel slag experiments to avoid introducing an additional silica source in the reactor. Zirconia beads were also preferred to stainless steel beads to avoid corrosion of the beads and contamination of the solid products. Each system requires different attrition-leaching conditions, and notably the properties of the beads (nature, density, size, and

hardness) were adapted to the reactor used. This study focuses on the influence of attrition-leaching on the chemical reactions and potential passivation, without investigating the nature of the beads and the influence it can have on the reactions for each different system, which is beyond the scope of this study and would require additional experiments.

The chemicals used for chalcopyrite dissolution were sulfuric acid (95 wt%, VWR international) and hydrogen peroxide (30 wt%, VWR international). For

BM Ni-MH leaching, sulfuric acid was diluted in deionized water ($0.05 \mu\text{S}/\text{cm}$) to reach a concentration of 4.0 M. In the case of slag carbonation, the source of protons was the dissolution of CO_2 into water.

2.2. Experimental reactors and analytical protocols

Two different leaching reactors with a similar operating principle were used (Figure 3): (1) loading of water and the beads into the reactor vessel, start of stirring and setting the experimental conditions of pressure, temperature and possibly pH, redox potential (E_h) and CO_2 pressure; (2) loading of the material to be leached, marking the start of the reaction; (3) maintaining all conditions constant during the reaction time; (4) end of the reaction by stopping the stirring, cooling, emptying the reactor and separating the beads from the suspension by sieving. The different experimental configurations tested in this study were: leaching only—without beads (L), attrition by particle pre-grinding followed by leaching (A-L), and concomitant attrition and leaching, referred to as attrition-leaching (AL). The particle pre-grinding was carried out in the same reactor as the leaching, at similar loading and stirring rate (see below), but only with water and beads, for 24 h for ferromagnetic slag and 3 h for chalcopyrite materials, relative to the difference in material hardness.

The operating conditions of the three chemical systems used in this study are presented in Table 2. It should be noted that the glass reactor was designed for industrial level scalability. For chalcopyrite concentrate experiments, the suspension was 3.25 wt% by mass, and for BM Ni-MH experiments the suspension was 1–10 wt%. Various amounts (from 0.25 to 3 kg) of 1 mm glass beads were introduced in the reactor yielding a filling rate of 3–10 vol%. The reactor was equipped with a four-blade Teflon stirrer and a torque meter (MK2 ETH model, PM Instrumentation) to measure torque and rotational speed. No baffles were present in the reactor because the creation of a vortex was desired to increase the contact between the material and the beads. A cryostat (AC200, Thermofisher) was used to maintain a uniform temperature by circulating water through the double jacket. The mechanical stirrer was set at ~ 560 rpm during the experiments. A platinum temperature

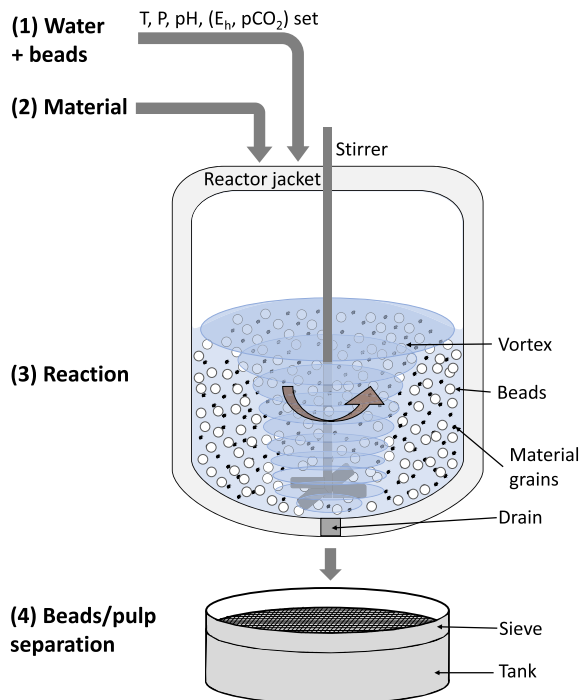


Figure 3. Schematic of an attrition-leaching (AL) experiment, showing the successive steps (1–4) of the experiment.

probe (Pt100 Duplex Probe, TC Direct) and a combined pH electrode (LL-Unitrode SC, Metrohm) were immersed in the solution to measure the temperature and pH, respectively, throughout the reaction. The combined pH electrode was protected by a thin SS grid to prevent the glass beads from damaging the probes. The pH was regulated using an automatic titrator (Titrand, Metrohm) by adding H_2SO_4 . The installation was connected to a computer which displayed and recorded the temperature, torque and stirring rate every minute. The acquisition and regulation of pH were carried out by the Tiamo software (at 0.1 Hz). The leaching rate for chalcopyrite and BM Ni-MH was measured by sample analysis of dissolved metal concentrations in the solution and by on-line monitoring of acid consumption. During a test run, the slurry was sampled with a 0.8 mm tube to prevent picking up beads. The sampled slurry was then filtered through a $0.25 \mu\text{m}$ syringe filter and the leachate samples obtained were analyzed by inductively coupled plasma-optical emission spectroscopy (ICP-OES; PerkinElmer Optima 8300) for the

Table 2. Operating parameters of the three chemical systems

System	Reactor material	V_{reactor} (L)	T (°C)	P (bar)	pH	E_h (mV vs SHE)	Stirring rate (rpm)	Beads material	Reference
Ferronickel slags	Stainless steel (peek liner)	0.3	150	10 (CO ₂)	5	—	500	Yttriated zirconia	[20]
Chalcopyrite	Glass	6	42	1	1.3	700	556	Glass	[15]
BM Ni-MH	Glass	6	40	1	1.0	—	560	Glass	This study

quantification of Cu, Ni, La, K and Na. The leaching yield $Y_{i(t)}^L$ (%) for the species at the time t of the experiment was obtained from the analysis of the liquid samples:

$$Y_{i(t)}^L (\%) = \frac{c_{m,i}(t) \cdot V_{\text{tot}}(t)}{m^0 \omega_i^0} \quad (8)$$

where $c_{m,i}(t)$ is the concentration of species i in the leachate sample at the time t , m^0 is the initial mass of the material, ω_i^0 is the mass fraction of species i in the starting material, and $V_{\text{tot}}(t)$ is expressed as:

$$V_{\text{tot}}(t) = V_{\text{H}_2\text{O}} + V_{\text{H}_2\text{SO}_4}(t) + V_{\text{H}_2\text{O}_2}(t) - \sum_{i=1}^{n(t)} V_{\text{sample},i} \quad (9)$$

where $V_{\text{H}_2\text{O}}$ is the initial volume of water added into the reactor, $V_{\text{H}_2\text{SO}_4}(t)$ is the volume of sulfuric acid added into the reactor at time t , $V_{\text{H}_2\text{O}_2}(t)$ is the volume of hydrogen peroxide added into the reactor at time t , $V_{\text{sample},i}$ is the volume of sample i and $n(t)$ is the number of samples at time t . Solid samples were also collected during the experiments for analysis. The beads were separated from the slurry at the end of each test run using an 850 μm RETSCH SS sieve. For BM Ni-MH experiments, 40 mL slurry samples were taken from the reactor during the experiment and the solid was then recovered in 2 different ways: (i) by solid filtration through a Büchner funnel with 0.2 μm filters (Whatman, mixed cellulose ester); (ii) by centrifugation (SIGMA Laboratory Centrifuges) at 6000 rpm for 5 min. In each case, the solid was then rinsed with 10 mL of deionized water to remove the residual leaching solution in the filter cake. Further details of the reactor and experimental protocol used for chalcopyrite experiments has been elaborated in Dakkoune [15]. In the carbonation experiments with ferronickel slags, leaching of Mg was followed indirectly by measuring the CO₂ consumption resulting from the rapid carbonation reaction between Mg^{2+} and aqueous HCO_3^- species. Further

details of the reactor and experimental protocol used has been elucidated in Dufourny [20].

A scanning electron microscope-field emission gun (SEM-FEG, JEOL JSM 7100F) equipped with an energy dispersive X-ray analyzer (EDX, Oxford ASDD X-Max detector) was used for particle observation, with an accelerating voltage of 10 kV and a working distance of 10 mm. The particle size distribution (PSD) was obtained by laser diffraction in wet dispersion mode using a Malvern Mastersizer 3000. Slurry samples were taken from the glass reactor in the same manner as liquid samples, but without filtration, and were diluted in deionized water to quench the reaction. For analysis of solids, we set the refractive index at 1.52, the absorption at 0.1 and the stirring rate at 1800 rpm. Five successive analyses were carried out for each sample.

The operating conditions used for these experiments are shown in Table 3. These conditions were chosen independently for each system to achieve sufficiently high reaction yields with leaching only mode. Temperature of 150 °C and CO₂ pressure of 10 bar used for carbonation of ferronickel slags were chosen to overcome the thermodynamic limitations of carbonation reaction [12]. Temperature of 42 °C for chalcopyrite leaching experiments was chosen to be compatible with bioleaching conditions [45]. Temperature for BM Ni-MH was set below the optimized temperature of 60 °C [46,47], to permit observation of potential effects of concomitant attrition and leaching on the reactions' kinetics and yields, as both increase with temperature.

3. Results and discussion

3.1. Yields and kinetics of reactions

As illustrated in Figure 4 and Table 3, the presence of beads in the reactor has a significant effect on the

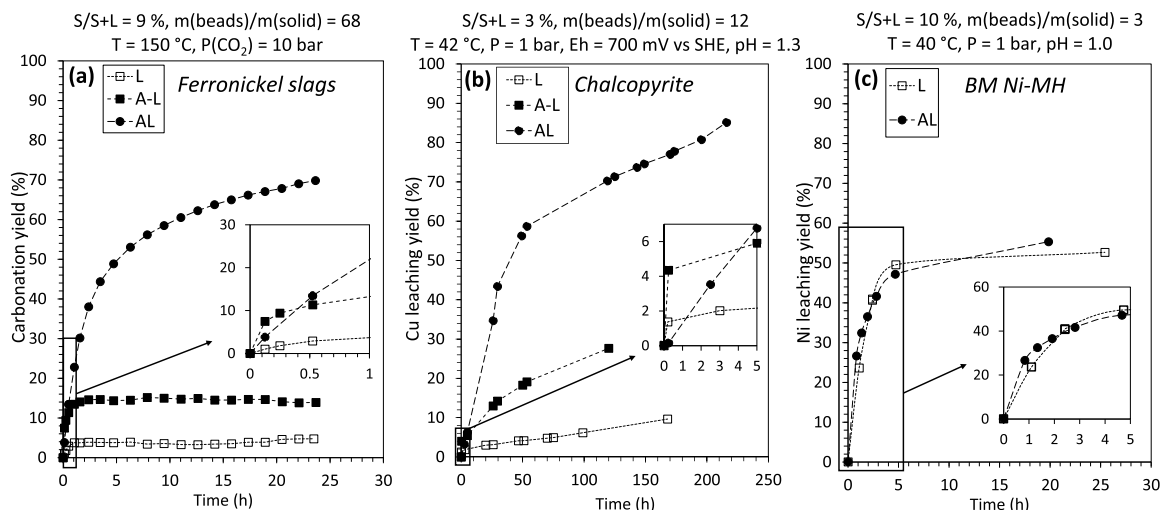


Figure 4. Reaction yields of reference (leaching only, L), two-step (attrition followed by leaching, A-L) and concomitant (attrition-leaching, AL) processes for ferronickel slag carbonation (a), chalcopyrite leaching (b) and BM Ni-MH leaching (c). Experimental data for ferronickel slag and chalcopyrite are taken from Dufourny [20] and Dakkoune [15], respectively.

Table 3. Summary of leaching experiments performed on ferronickel slags, chalcopyrite and BM Ni-MH

Material	Initial configuration				Final configuration		
	m_{solid} (g)	m_{beads} (g)	S/S + L initial (wt%)	Solid fraction (μm)	Time (h)	H ⁺ (mol)	H ₂ O ₂ (mol)
<i>Ferronickel slag</i> ^a							
FS 1-L	8.0	—	9.1	<100	24	—	—
FS 1-A-L	8.1	—	9.4	<100	24	—	—
FS 1-AL	8.2	540	9.3	<100	24	—	—
<i>Chalcopyrite</i> ^b							
Ch-L	84	—	3.3	<200	96	0.1	0.08
Ch-A-L	84	—	3.3	<200	120	0.8	0.9
Ch-AL	84	1000	3.3	<200	216	1.2	1.5
<i>BM Ni-MH</i>							
BM2-L	306	—	10.0	<100	25	5.5	—
BM3-AL	298	1000	10.4	<100	20	5.8	—
BM4-L	30	—	1.2	<100	24	0.7	—
BM5-AL	30	1000	1.2	<100	22	0.7	—
BM6-AL	305	3000	9.7	<100	53	5.9	—
BM7-L	100	—	3.7	<100	20	1.8	—
BM8-AL	100	1000	3.8	<100	22	1.7	—
BM9-L	100	—	3.8	100–500	21	2.1	—
BM10-AL	100	1000	3.9	100–500	21	1.8	—

^aData taken from [20].

^bData taken from [15].

carbonation yield of ferronickel slags (Figure 4a) and on chalcopyrite dissolution (Figure 4b). However, this effect is negligible on Ni dissolution yield from BM Ni-MH (Figure 4c), where the Ni extraction yield is the same with the AL and L modes, reaching only ~50% after 20 h.

Several experimental conditions (size fraction, S/S+L ratio, amount of beads) have been investigated in BM Ni-MH leaching experiments, but the extraction yield always remained very similar, in the range 50–70% (Figure 5). Such yields are quite low compared to other Ni dissolution yields reported in literature at a similar pH of 1 (>80%; [24,46]). It is hypothesized that production (including thermal treatment) and storage conditions (long term storage in air) [23] may account for the yield variations of comparable BM Ni-MH materials due to the existence of Ni in two redox states and several phases (see Table 1), including a difficult-to-leach oxide phase [46].

Reaction kinetics are very different for the three systems used in our study. If we consider the reaction as a whole, in the case of ferronickel slags, the reaction stopped after ~2 h in L and A-L modes, while the yield increases and reaches a plateau after ~20 h in AL mode (Figure 4a). For chalcopyrite leaching, the kinetics are higher in the first 50 h of reaction for the AL mode, reaching a 60% Cu extraction yield. Furthermore, even if the yield continues to increase with time for the three modes, the highest dissolution rate is with the AL mode (Figure 4b). For BM Ni-MH leaching, as mentioned earlier, the kinetics are globally similar for L and AL modes and the dissolution rate starts to decrease after ~5 h.

If we consider the first instants of the reactions for the three materials (plotted in the inserts of Figure 4a–c), we can observe some similarities. During the initial moments of the reactions, AL mode exhibits a higher dissolution rate than L mode for all materials, including BM Ni-MH (Figure 4a–c). In the experiments with ferronickel slags and chalcopyrite, the kinetics of A-L mode are initially higher than that of AL mode (Figure 4a,b), due to preliminary grinding resulting in enhanced reactive surface area. After 20 min for carbonation and 5 h for Cu leaching, the AL mode leads to faster kinetics. As discussed in previous studies [15,20], the formation of passivation layers quickly limits the reaction in the A-L mode, while these layers are peeled off in AL mode. AL mode

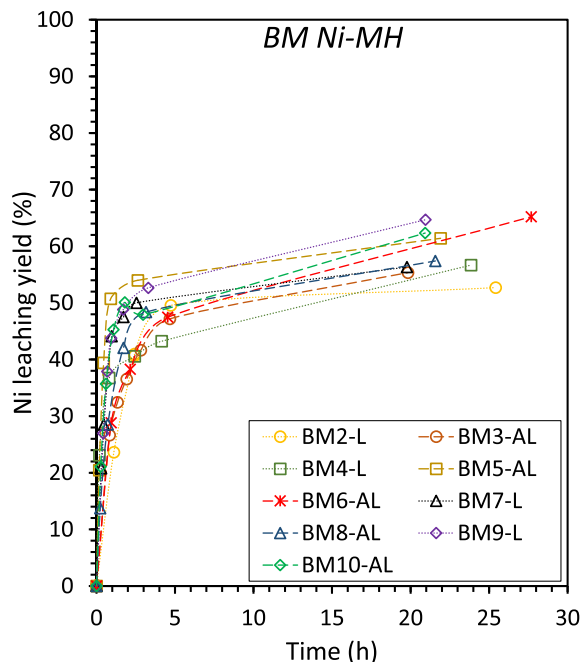


Figure 5. Leaching yields of Ni in aqueous H_2SO_4 solution at pH 1.0, $T = 40^\circ\text{C}$, $P = 1$ bar for BM Ni-MH leaching experiments, with different solid fractions (<100 and 100–500 μm), S/S+L ratios (1–10%), and amounts of beads (1–3 kg). Experimental conditions for each run are detailed in Table 3.

ability to depassivate particles during the reaction is the main advantage of *in situ* attrition compared to the mechanical activation implemented before the addition of the reactant in the A-L mode. It is important to note that each material presents its own characteristics, resulting in different choices of operating conditions (size fraction, S/S+L ratio, and amount of beads), as illustrated in Figure 4. Furthermore, parameters such as the ratio $m(\text{beads})/m(\text{solid})$ and S/S+L were investigated for the BM Ni-MH in this study, and the kinetics and yields (Table 3 and Figure 5) were similar.

Regarding leaching of BM Ni-MH, we analyzed the progression of acid consumption (thanks to 0.1 Hz monitoring) to better follow reaction kinetics during the initial 2-h period of leaching (see Figure 6). We assumed that acid consumption was proportional to the concentration of Ni in the aqueous phase,

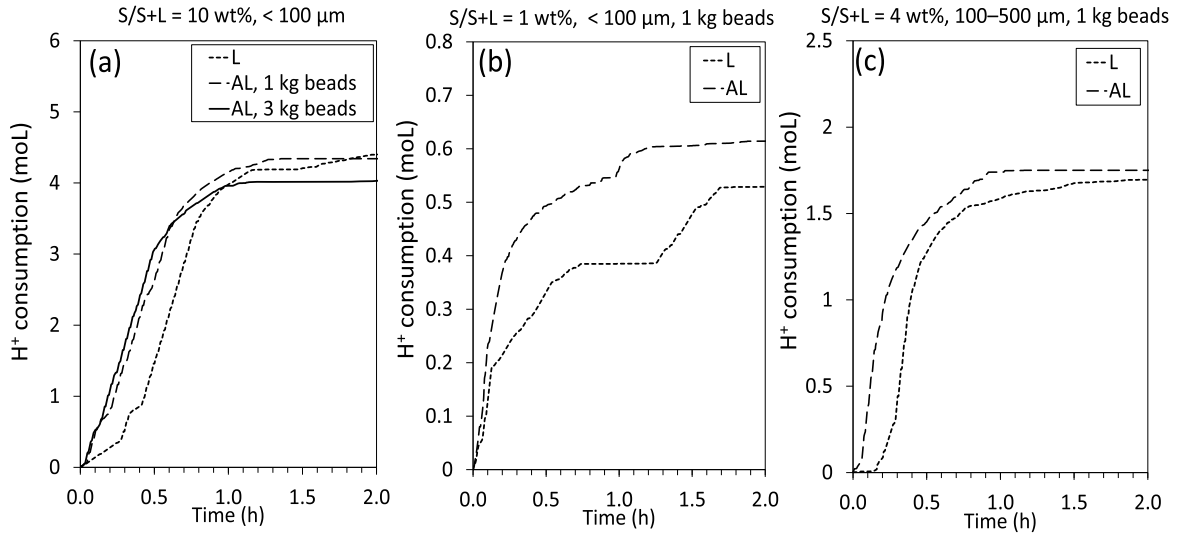
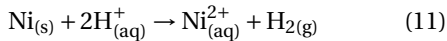
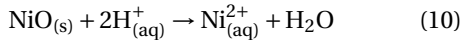


Figure 6. Acid consumption during the early stage of BM Ni-MH leaching experiments, with (L; leaching) and without beads (AL; attrition-leaching), for the size fraction $<100\ \mu\text{m}$ with $\text{S/S+L} = 10\ \text{wt}\%$ (a) and $\text{S/S+L} = 1\ \text{wt}\%$ (b) and for the size fraction $100\text{--}500\ \mu\text{m}$ with $\text{S/S+L} = 4\ \text{wt}\%$ (c).

as determined by the main dissolution reactions:



Based on data, it can be inferred that the dissolution reaction is faster with attrition-leaching than leaching only in the first hour, whatever the size fraction used (<100 or $100\text{--}500\ \mu\text{m}$, Figure 6b,c). Additionally, using a larger amount of beads (1 kg or 3 kg of beads, Figure 6a) did not show any impact.

3.2. Particle size distribution

Particle size was investigated for each system, based on the Malvern's PSD measurements and direct SEM observations of the particles recovered at the end of the experiments or sampled during the runs. For the three materials, SEM micrographs at the end of the experiments show that large grains ($>10\ \mu\text{m}$) are still present in the L mode experiments (Figure 7a,c,e), and the particles consisted of agglomerates ($5\text{--}50\ \mu\text{m}$) of very fine grains ($<100\ \text{nm}$) in the AL mode experiments (Figure 7b,d,f). The AL mode thus led to the formation of a large quantity of particles with a mean size below $1\ \mu\text{m}$, while the initial size was $\sim 50\ \mu\text{m}$.

As dissolution reactions are surface dependent, particle surface area distribution was estimated from the measured particle volume distribution (Figure 8a–c). The distributions were deconvoluted for similar reaction times (20–26 h) for the three materials by using a combination of 2 lognormal distributions $f_i(x)$ as shown below:

$$f(x) = \lambda f_1(x) + (1 - \lambda) f_2(x) \quad (12)$$

where $x = \text{Lognormal}(\mu_i, \sigma_i)$

where μ_i is the mean value and σ_i is the standard deviation of the i th lognormal distribution and λ is the proportion of the first distribution. The deconvolution with 2 lognormal distributions was deemed sufficient as it was clearly seen in most cases and it fitted rather well the particle surface area distributions at all selected reaction times for all three materials. As illustrated in Figure 8a–c, a significant size change occurred during the attrition-leaching process with the occurrence of a bimodal distribution for the three materials. The first mode (mode 1) corresponds to small agglomerates ($0.5\text{--}0.7\ \mu\text{m}$) that are likely due to the binding of smaller particles ($<100\ \text{nm}$), which is evidenced in the SEM pictures for the three materials (Figure 7b,d,f). The second mode (mode 2) corresponds to medium sized agglomerates ($\sim 1\text{--}10\ \mu\text{m}$). Initially, they include the original particles which are

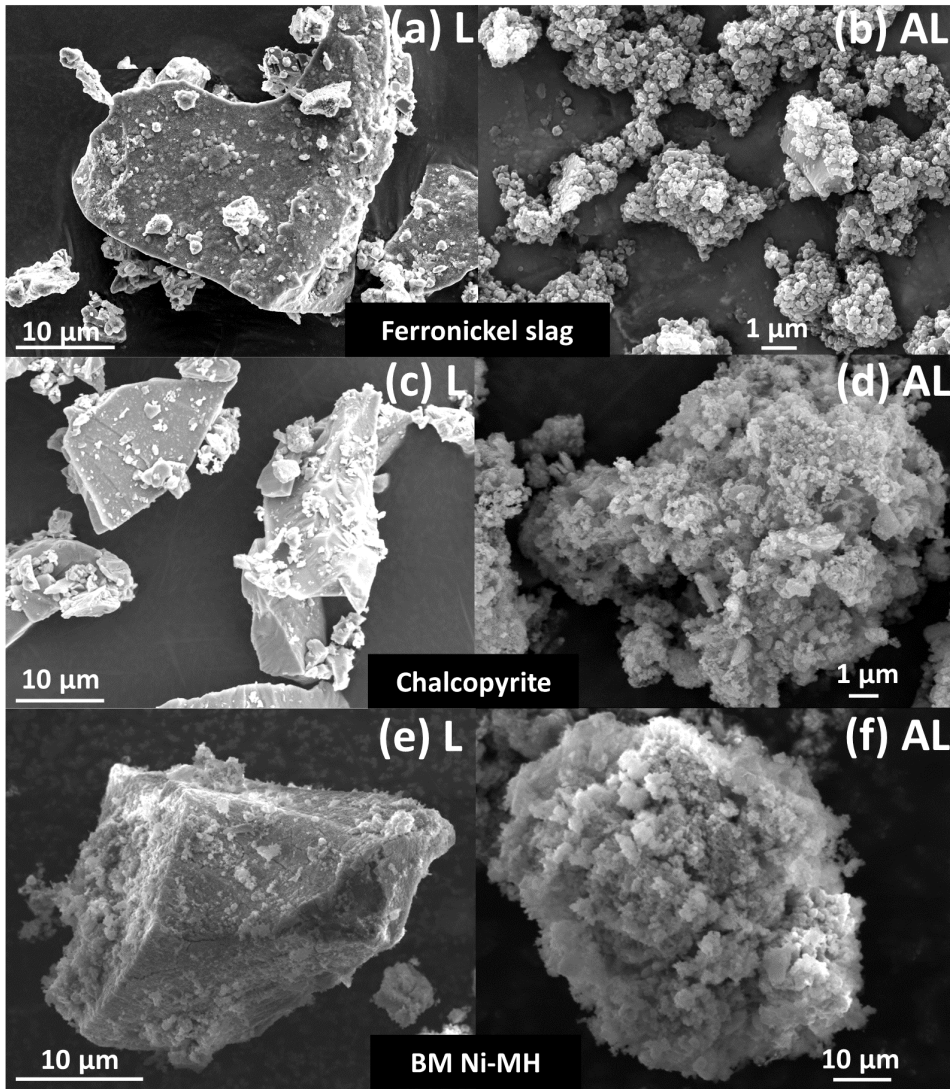


Figure 7. SEM micrographs of: ferronickel slag ($<100 \mu\text{m}$) after leaching (a) and attrition-leaching (540 g of 1 mm beads) (b), at 150°C , $P(\text{CO}_2) = 10 \text{ bar}$, $t = 24 \text{ h}$; raw chalcopyrite concentrate (c) and after 168 h of attrition-leaching (500 g of beads) (d) at $\text{pH} = 1.3$, $E_h = 700 \text{ mV vs SHE}$, $T = 42^\circ\text{C}$, $t = 168 \text{ h}$; BM Ni-MH ($<100 \mu\text{m}$) after leaching (e) and attrition-leaching (1 kg of beads) (f) at $\text{pH} = 1.0$, $T = 40^\circ\text{C}$, $t = 24 \text{ h}$.

eventually subjected to abrasion and/or dissolution over time. In Figure 8b,c it can be seen that the proportion of the first mode compared to the second mode increases through time for chalcopyrite and BM Ni-MH materials. The particle size of the second mode also decreases through time, with a more pronounced effect for BM Ni-MH than for chalcopyrite. On the contrary, the proportion between these two

modes is quite constant for the experiments with ferronickel slags.

As schematized in Figure 9, our hypothesis to explain the formation of such similar agglomerates in each system is that a balance between the agglomeration of small particles and the breakage of large agglomerates is taking place. At the very beginning of the attrition-leaching process (between $t = 0 \text{ h}$ and

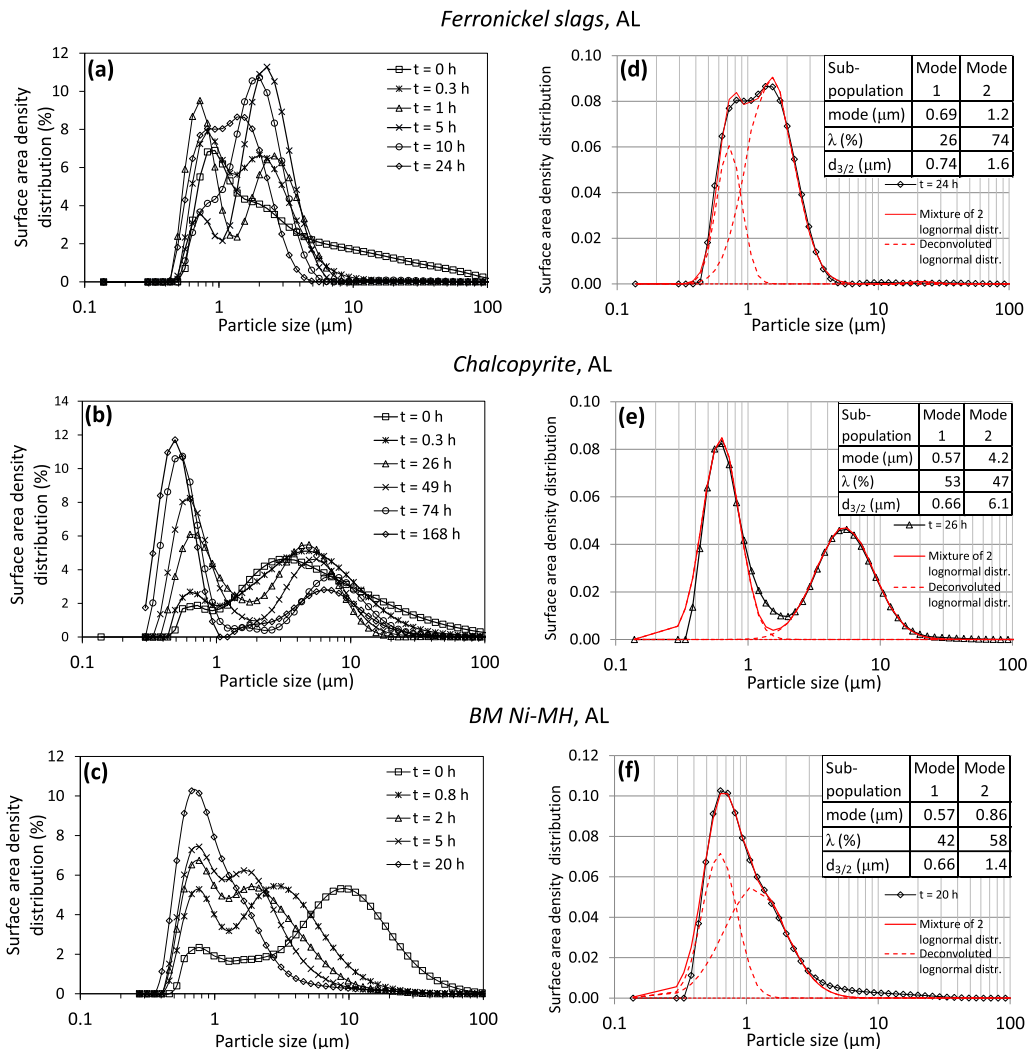


Figure 8. Surface area density distribution of particles sampled from the reactor at different reaction times during attrition-leaching (AL) of ferronickel slags (a), chalcopyrite (b) and BM Ni-MH (c), and their respective PSD surface deconvolution (d), (e) and (f), with corresponding distribution parameters, for similar reaction times (20–26 h).

$t = 0.3$ – 0.8 h), the particles larger than $10 \mu\text{m}$ are fragmented, leading to their disappearance, as can be seen in surface area density distribution of Figure 8a–c. It is worth noting that the first mode is very similar for the three materials, while the second mode differs significantly, highlighting a possible influence of the materials' nature on the breaking efficiency of the beads and on the cohesion of the nanometer-sized grains together to form more or less resistant agglomerates.

The following steps illustrate the successive and continuous synergistic mechanisms during the attrition-leaching process (Figure 9): (i) comminution increases the specific surface area; (ii) if a passivation layer forms, it is removed from the particle surface by attrition; (iii) re-agglomeration of the particles, leading to a decrease in the reactive surface and/or to diffusional effects; (iv) the re-agglomerated particles reach a size limit as they are partially fragmented by the beads.

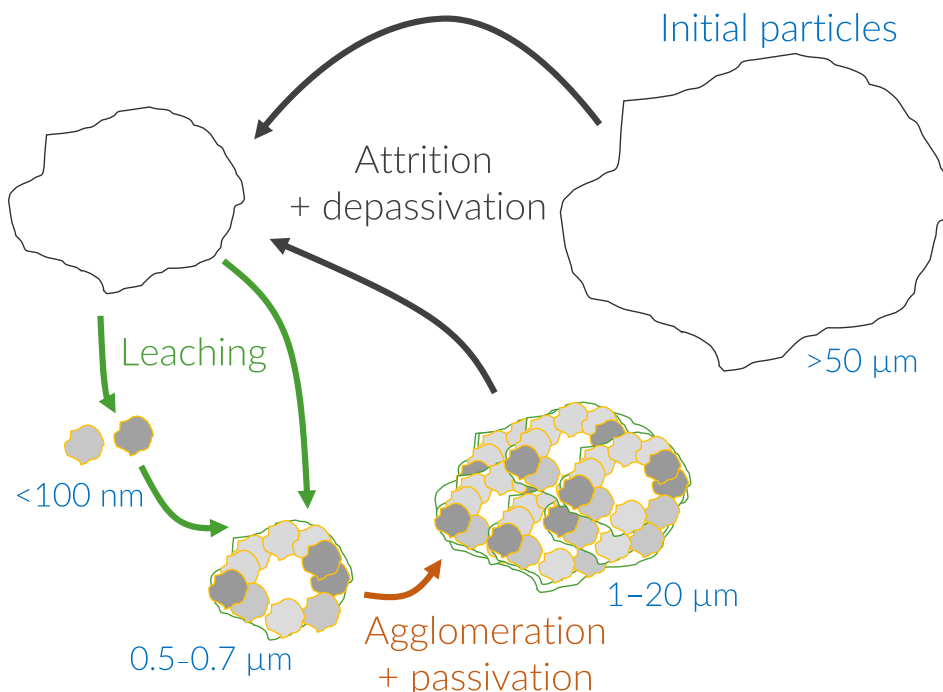


Figure 9. Scheme of concomitant particles' attrition and agglomeration to explain the particle size distribution and multi-scale aggregates.

3.3. A material-dependent synergy

Although the three processes considered in this work occur at different reaction timescales due to their chemical differences, the combination of leaching and attrition significantly enhances the extraction yields of both ferronickel slag carbonation and chalcopyrite leaching. Conversely, in the case of BM Ni-MH, no quantitative effect of attrition-leaching on the time-extraction yield of Ni was observed compared to leaching only (Figure 4 and Table 3). No particular effect of the amount of beads (1 or 3 kg of beads) or S/S+L ratio on the BM Ni-MH dissolution yield was observed either (Table 3). Nevertheless, similar attrition and particle breakage mechanism was observed for the three materials (Figure 8), as confirmed by the similarity of their PSD modes. The observed synergy in the attrition-leaching mode is a complex phenomenon likely caused by the continuous attrition of the reactive surface. An observation by transmission electron microscopy (TEM) of thin sections prepared with a focused ion beam (FIB) by Dufourny [20] showed that a potential source of the attrition-leaching synergy is the continuous de-

passivation of the reaction front. It was also found that the ratio of micropore to mesopore volume was 4 times lower for AL mode than for A-L and L modes, showing that the specific surface area also controls the kinetics and yields of the reaction.

In the case of BM Ni-MH material, we expected the porous insoluble layers to hinder the reaction rate. However, as attrition-leaching was only marginally beneficial to the dissolution of Ni in the initial moments of reaction due to particle grinding, our work showed that there was no passivation of BM grains, and thus the limitation in Ni leaching yield is due to other causes. The precipitation of potassium-REE double sulfate salts $\text{KREE}(\text{SO}_4)_2 \cdot \text{H}_2\text{O}_{(\text{s})}$ (see Equation (7)) may be responsible for Ni leaching inhibition. Such precipitation reaction takes place at high S/S+L ratios, when REE concentrations reach the solubility limit of the salts. As shown in Figure 10, we reached the REE solubility limit in some of our experiments, when the initial S/S+L was equal to 10 wt%, with a simultaneous decrease in La and K leaching yields in the fluid. The La extraction yields then remained below 40% after 5 hours of reaction, while La extraction yields were >70% with S/S+L

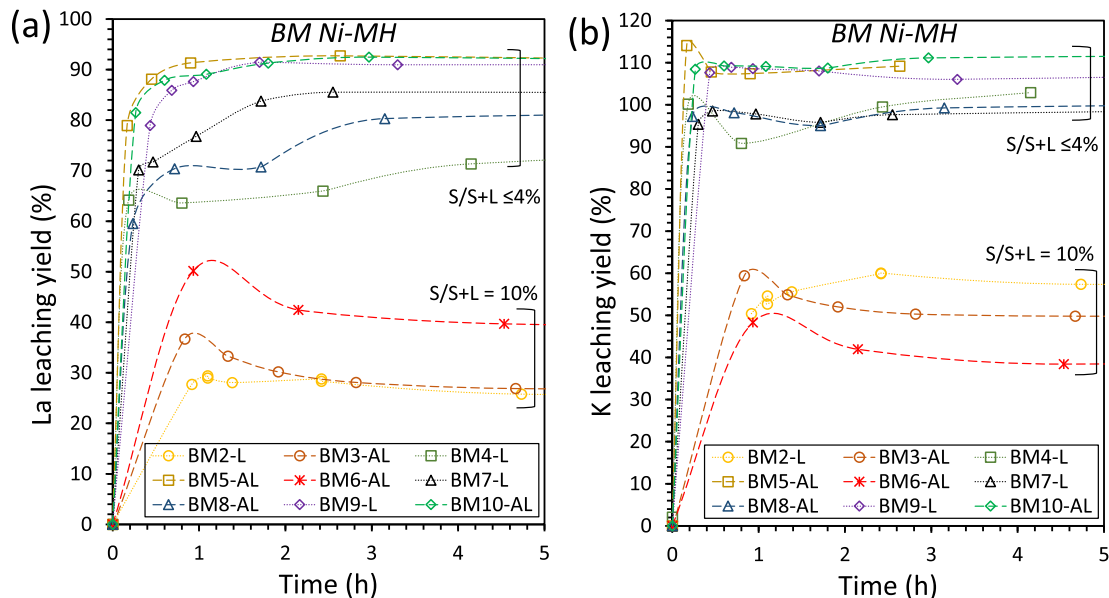


Figure 10. Leaching yields of La (a) and K (b) in aqueous H_2SO_4 solution at pH 1.0, $T = 40^\circ\text{C}$, $P = 1$ bar for BM Ni-MH leaching experiments. Experimental conditions for each run are detailed in Table 3. At $\text{S/S+L} = 10\%$ the double sulfate $\text{KREE}(\text{SO}_4)_2 \cdot \text{H}_2\text{O}_{(\text{s})}$ precipitates. K leaching yields above 100% are due to a light leak from the pH electrode (filled with KCl 3 M).

ratios of 4 wt% and 1 wt%. However, the precipitation of La did not interfere with the Ni dissolution yields as shown in experiments with S/S+L ratios of 10% (BM2-L, BM3-AL and BM6-AL) plotted in Figure 5, which have similar Ni dissolution yields than other experiments with S/S+L ratios lower than 4%. Furthermore, in the case of REE salts precipitation, the La extraction yields are similar for both AL and L modes with an S/S+L ratio of 10% (BM2-L and BM3-AL; Figure 10a). Since the presence of beads has no significant effect on the extraction yields of Ni, with and without REE salts precipitation, the limiting mechanisms are thus not related to diffusion through surface layers. Other hypotheses must be investigated to explain the limited Ni dissolution yield, which may be due to chemical limitations, such as limited dissolution of the different Ni phases in the black mass, specifically the nickel metal and the nickel oxide [23,46].

4. Conclusions and perspectives

Attrition-leaching is a simple and widely-applicable mechanochemical method for investigating leaching

reaction hindered by the formation of surface layers. In this study, the cases of three different materials were compared: ferronickel slags and chalcopyrite concentrates on one hand, using data from previous works, and BM Ni-MH on the other hand, based on a dedicated experimental study. The comparison shows that, at the very beginning of the reaction, the kinetics of the attrition-leaching process increases compared to leaching only, for all three materials. This is very likely due to the increase in reactive surface provoked by particles fragmentation. However, the subsequent influence of attrition on the yield depends directly on the material considered: in the case of ferronickel slag and chalcopyrite, a high gain is obtained with concomitant attrition, while in the case of BM Ni-MH there is no improvement.

Attrition-leaching appears to involve a synergistic mechanism that relies on the continuous abrasion of the surface layer. This layer can be a genuine passivation layer formed *in situ*, during the leaching reaction, due to the poor solubility of some secondary compounds, as in the case of ferronickel slag or chalcopyrite materials. It can also consist of an insoluble porous layer, as in the case of BM Ni-MH,

that does not control the leaching rate. The PSD analyses showed that, despite their very different leaching behavior, the three materials exhibited similar fragmentation effects, with comparable particle size distribution modes observed after sustained attrition. Furthermore, we showed that carrying out the leaching reactions in AL mode has a great potential to be studied further, including the potential mechano-chemical activation of refractory minerals, whose leaching may be inhibited by the formation of a passivation layer.

It is also important to note that attrition leaching experiments considered in this study were not optimized in terms of energy consumption. Indeed, the continuous energy-intensive agitation of the beads contained in the reactors lead to significant energy consumptions (e.g. 3.3 kWh/m³ for the glass reactor with 1 kg of glass beads). Therefore, if reaction times remain long, improvement of the system's efficiency and reduction of its energy consumption are required, for instance by utilizing a combination of short attrition-leaching steps and longer leaching only steps (e.g. [33]).

Acronyms

BM	Black mass
Ni-MH	Nickel-metal hydride
L	Leaching only
A-L	Attrition followed by leaching
AL	Attrition-leaching
S/S+L	Solid to liquid ratio
PSD	Particle size distribution

Declaration of interests

The authors do not work for, advise, own shares in, or receive funds from any organization that could benefit from this article, and have declared no affiliations other than their research organizations.

Funding

This work was funded by the French National Research Agency project BIOMECALIX (Grant No. ANR-18-CE07-003101), project Carmex (Grant No. ANR-08-PCO2-002), the New Caledonian Energy Agency

ACE (Grant No. CS17-3160-00) and the French Environment and Energy Management Agency ADEME (Grant No. 1894C0021).

Acknowledgments

We thank Boliden for the supply of chalcopyrite concentrate and we thank SNAM Group for the supply of black mass powder prepared from Ni-MH batteries. We also thank BRGM for collaboration with A.-G. Guezennec. The authors acknowledge the technical support at LGC Toulouse of M.-L. De Solan Bethmale, C. Rey-Rouch and A. Moreau for their contribution to chemical analyses and solid characterization. The contribution of J.-L. Labat, M. Riedel, L. Farhi, and Q. Ribière for the design and assembly of the experimental setup is gratefully acknowledged.

References

- [1] K. Binnemans, P. T. Jones, *J. Sustain. Metal.*, 2023, **9**, 1-25.
- [2] F. Faraji, A. Alizadeh, F. Rashchi, N. Mostoufi, *Rev. Chem. Eng.*, 2022, **38**, 113-148.
- [3] Q. Tan, J. Li, *Environ. Sci. Technol.*, 2015, **49**, 5849-5861.
- [4] O. S. Odebiyi, H. Du, B. Liu, S. Wang, *J. Sustain. Metal.*, 2022, **8**, 1393-1421.
- [5] J. Li, M. Hitch, *Miner. Eng.*, 2018, **128**, 69-83.
- [6] J. Pronost, G. Beaudoin, J. Tremblay, F. Larachi, J. Duchesne, R. Hébert, M. Constantin, *Environ. Sci. Technol.*, 2011, **45**, 9413-9420.
- [7] A. B. Ghacham, L.-C. Pasquier, E. Cecchi, J.-F. Blais, G. Mercier, *Environ. Sci. Pollut. Res.*, 2016, **23**, 17635-17646.
- [8] A. Ben Ghacham, L.-C. Pasquier, E. Cecchi, J.-F. Blais, G. Mercier, *J. Cleaner Prod.*, 2017, **166**, 869-878.
- [9] S. Ó. Snæbjörnsdóttir, B. Sigfússon, C. Marieni, D. Goldberg, S. R. Gislason, E. H. Oelkers, *Nat. Rev. Earth Environ.*, 2020, **1**, 90-102.
- [10] N. Thonemann, L. Zacharopoulos, F. Fromme, J. Nühlen, *J. Cleaner Prod.*, 2022, **332**, article no. 130067.
- [11] P. Baláz, M. Achimovičová, *Hydrometallurgy*, 2006, **84**, 60-68.
- [12] C. Julcour, F. Bourgeois, B. Bonfils, I. Benhamed, F. Guyot, F. Bodéan, C. Petiot, É. C. Gaucher, *Chem. Eng. J.*, 2015, **262**, 716-726.
- [13] C. Julcour, L. Cassayre, I. Benhamed, J. Diouani, F. Bourgeois, *Front. Chem. Eng.*, 2020, **2**, article no. 588579.
- [14] G. Rim, D. Wang, M. Rayson, G. Brent, A.-H. A. Park, *Indust. Eng. Chem. Res.*, 2020, **59**, 6517-6531.
- [15] A. Dakkoune, F. Bourgeois, A. Po, C. Joulain, A. Hubau, S. Touzé, C. Julcour, A.-G. Guezennec, L. Cassayre, *ACS Eng. Au*, 2023, **3**, 195-209.
- [16] G. S. Anderson, P. A. Bandarian, *Miner. Eng.*, 2019, **132**, 211-219.
- [17] F. Bodéan, F. Bourgeois, C. Petiot, T. Augé, B. Bonfils, C. Julcour-Lebigue, F. Guyot, A. Boukary, J. Tremosa, A. Lassin, E. C. Gaucher, P. Chiquet, *Miner. Eng.*, 2014, **59**, 52-63.

- [18] F. Bourgeois, P. Laniesse, M. Cyr, C. Julcour, *Front. Energy Res.*, 2020, **8**, article no. 113.
- [19] F. Gao, Z. Huang, H. Li, X. Li, K. Wang, M. F. Hamza, Y. Wei, T. Fujita, *J. Cleaner Prod.*, 2021, **303**, article no. 127049.
- [20] A. Dufourny, C. Julcour, J. Esvan, L. Cassayre, P. Laniesse, F. Bourgeois, *Front. Clim.*, 2022, **4**, article no. 946735.
- [21] A. Ghahremaninezhad, D. G. Dixon, E. Asselin, *Electrochim. Acta*, 2013, **87**, 97-112.
- [22] M. Kartal, F. Xia, D. Ralph, W. D. A. Rickard, F. Renard, W. Li, *Hydrometallurgy*, 2020, **191**, article no. 105192.
- [23] M. Zielinski, L. Cassayre, P. Destrac, N. Coppey, G. Garin, B. Biscans, *ChemSusChem*, 2020, **13**, 616-628.
- [24] L. Cassayre, B. Guzhov, M. Zielinski, B. Biscans, *Renew. Sustain. Energy Rev.*, 2022, **170**, article no. 112983.
- [25] F. Abdul, A. Iizuka, H.-J. Ho, K. Adachi, E. Shibata, *Environ. Sci. Pollut. Res.*, 2023, **30**, 78041-78074.
- [26] D. Daval, O. Sissmann, N. Menguy, G. D. Saldi, F. Guyot, I. Martinez, J. Corvisier, B. Garcia, I. Machouk, K. G. Knauss, R. Hellmann, *Chem. Geol.*, 2011, **284**, 193-209.
- [27] F. Farhang, T. K. Oliver, M. S. Rayson, G. F. Brent, T. S. Molloy, M. Stockenhuber, E. M. Kennedy, *J. CO₂ Util.*, 2019, **30**, 123-129.
- [28] G. M. O'Connor, J. J. Eksteen, *Miner. Eng.*, 2020, **154**, article no. 106401.
- [29] C. Lv, H. Wu, W. Lin, J. B. Illerup, A. P. Karcz, S. Ye, A. J. Damø, *Hydrometallurgy*, 2019, **188**, 22-30.
- [30] R. P. Hackl, D. B. Dreisinger, E. Peters, J. A. King, *Hydrometallurgy*, 1995, **39**, 25-48.
- [31] J. Li, N. Kawashima, K. Kaplun, V. J. Absolon, A. R. Gerson, *Geochim. Cosmochim. Acta*, 2010, **74**, 2881-2893.
- [32] Y. Li, B. Wang, Q. Xiao, C. Lartey, Q. Zhang, *Hydrometallurgy*, 2017, **173**, 149-155.
- [33] M. Mulligan, *J. South. Afr. Inst. Min. Metall.*, 2017, **117**, 741-747.
- [34] A. V. G. Chizmeshya, M. J. McKelvy, K. Squires, R. W. Carpenter, H. Bearat, *A Novel Approach to Mineral Carbonation: Enhancing Carbonation While Avoiding Mineral Pretreatment Process Cost*, Arizona State University, Tempe, AZ, 2007.
- [35] S. Chalouati, A. Yoosefdoost, Y. W. Chiang, R. M. Santos, *Int. J. Coal Geol.*, 2023, **277**, article no. 104332.
- [36] X. Ke, V. A. Baki, L. Skevi, *J. CO₂ Util.*, 2023, **68**, article no. 102367.
- [37] J. R. Cobble, C. E. Jordan, D. A. Rice, *Hydrometallurgical Production of Copper from Flotation Concentrates*, U.S. Department of the Interior, Bureau of Mines, 1993.
- [38] M. Minagawa, S. Hisatomi, T. Kato, G. Granata, C. Tokoro, *Adv. Powder Technol.*, 2018, **29**, 471-478.
- [39] G. Granata, K. Takahashi, T. Kato, C. Tokoro, *Miner. Eng.*, 2019, **131**, 280-285.
- [40] S.-T. Cao, X.-F. Zheng, Z.-Y. Nie, Y.-H. Zhou, H.-C. Liu, J.-H. Chen, H.-Y. Yang, J.-L. Xia, *Minerals*, 2020, **10**, article no. 788.
- [41] L. Mussapyrova, R. Nadirov, P. Baláž, M. Rajňák, R. Bureš, M. Baláž, *J. Mater. Res. Technol.*, 2021, **12**, 2011-2025.
- [42] A. Porvali, S. Ojanen, B. P. Wilson, R. Serna-Guerrero, M. Lundström, *J. Sustain. Metal.*, 2020, **6**, 78-90.
- [43] M. Zielinski, L. Cassayre, P. Floquet, M. Macouin, P. Destrac, N. Coppey, C. Foulet, B. Biscans, *Waste Manage.*, 2020, **118**, 677-687.
- [44] L. Cassayre, F. Bourgeois, C. Julcour-Lebigue, I. Benhamed, J. Diouani, K. Nahdi, *IMPC 2016: XXVIII International Mineral Processing Congress Proceedings*, Curran Associates, 2016, 1 pages.
- [45] A. Hubau, A.-G. Guezennec, C. Joulain, C. Falagán, D. Dew, K. A. Hudson-Edwards, *Hydrometallurgy*, 2020, **197**, article no. 105484.
- [46] M. Takano, S. Asano, M. Goto, *Hydrometallurgy*, 2022, **209**, article no. 105826.
- [47] A. M. A.-A. Otron, T. Millogo, L.-H. Tran, J.-F. Blais, *Environ. Technol.*, 2023, 1-13.